PNAS RESEARCH ARTICLE | MICROBIOLOGY
EARTH, ATMOSPHERIC, AND PLANETARY SCIENCES

Pathways of N_2O production by marine ammonia-oxidizing archaea determined from dual-isotope labeling

Xianhui S. Wan[a,1], Lei Hou[b,c], Shuh-Ji Kao[b], Yao Zhang[b], Hua-Xia Sheng[b], Hui Shen[b], Senwei Tong[b], Wei Qin[c], and Bess B. Ward[a,1]

Edited by Donald Canfield, Syddansk Universitet, Odense M, Denmark; received December 13, 2022; accepted February 7, 2023

The ocean is a net source of the greenhouse gas and ozone-depleting substance, nitrous oxide (N_2O), to the atmosphere. Most of that N_2O is produced as a trace side product during ammonia oxidation, primarily by ammonia-oxidizing archaea (AOA), which numerically dominate the ammonia-oxidizing community in most marine environments. The pathways to N_2O production and their kinetics, however, are not completely understood. Here, we use ^{15}N and ^{18}O isotopes to determine the kinetics of N_2O production and trace the source of nitrogen (N) and oxygen (O) atoms in N_2O produced by a model marine AOA species, *Nitrosopumilus maritimus*. We find that during ammonia oxidation, the apparent half saturation constants of nitrite and N_2O production are comparable, suggesting that both processes are enzymatically controlled and tightly coupled at low ammonia concentrations. The constituent atoms in N_2O are derived from ammonia, nitrite, O_2, and H_2O via multiple pathways. Ammonia is the primary source of N atoms in N_2O, but its contribution varies with ammonia to nitrite ratio. The ratio of $^{45}N_2O$ to $^{46}N_2O$ (i.e., single or double labeled N) varies with substrate ratio, leading to widely varying isotopic signatures in the N_2O pool. O_2 is the primary source for O atoms. In addition to the previously demonstrated hybrid formation pathway, we found a substantial contribution by hydroxylamine oxidation, while nitrite reduction is an insignificant source of N_2O. Our study highlights the power of dual ^{15}N-^{18}O isotope labeling to disentangle N_2O production pathways in microbes, with implications for interpretation of pathways and regulation of marine N_2O sources.

nitrous oxide | ammonia-oxidizing archaea | dual isotope | marine N_2O production pathways | kinetics

Ammonia-oxidizing archaea (AOA) are ubiquitous and abundant members of the marine plankton; they are almost exclusively responsible for ammonia oxidation in the world ocean (1, 2). Globally, over 80% of marine nitrous oxide (N_2O) is estimated to be produced as a side product of ammonia oxidation (3–5), indicating a dominant role of marine AOA in determining N_2O distribution and its flux from ocean to atmosphere. Compared to their bacterial counterparts, ammonia-oxidizing bacteria (AOB), marine AOA lack the genes encoding the known bacterial machineries for N_2O production (6) and exhibit lower N_2O yield (7–9), implying distinct mechanisms of N_2O production between AOA and AOB (10–12). The marine AOA demonstrate significantly higher affinity toward total ammonia (NH_3 plus NH_4^+, hereafter referred to as NH_4^+) for ammonia oxidation during nitrite (NO_2^-) production than AOB (2), but the cellular kinetics of N_2O production have not been explored. Hydroxylamine (NH_2OH) and nitric oxide (NO) have been identified as key intermediates in AOA metabolism (13–15), implying multiple potential pathways for N_2O production as both NH_2OH and NO are likely precursors of N_2O. However, the explicit pathways of archaeal N_2O production are still incompletely known and remain controversial (10–12). The hybrid N_2O formation pathway (in which the two N atoms in N_2O are derived from different sources via the abiotic reaction between NH_2OH and NO) has been experimentally demonstrated and is considered the dominant pathway for N_2O production in AOA cultures and natural environments (Fig. 1*A*) (10–12). Other AOA pathways may include N_2O production via NO_2^- reduction at low pH (16) and a novel NO dismutation pathway in marine AOA under anaerobic conditions (17). In contrast, no experimental evidence that AOA can directly convert NH_2OH to N_2O via NH_2OH oxidation, either enzymatically or abiotically, has been reported. It is important to determine which pathways occur during archaeal ammonia oxidation and which are relevant in various environmental conditions because 1) the pathway and rate of N_2O production might vary with NH_4^+ and NO_2^- availability, as both are involved in N_2O formation; and 2) different sources of N and O used by AOA to produce N_2O may impart distinct isotope signatures, which are used to deduce the sources of N_2O in natural and man-made systems.

Elucidation of all potential sources of N_2O, however, remains a challenging task. To date, most investigations on AOA N_2O production pathways have focused on the source

Significance

Ammonia-oxidizing archaea (AOA) are the major source of marine nitrous oxide (N_2O); however, the cellular kinetics and pathways of archaeal N_2O production remain unclear. We characterize N_2O production kinetics of a model marine AOA species *Nitrosopumilus maritimus* at low ammonia concentrations and quantify the relative contributions of multiple N_2O production pathways using dual ^{15}N-^{18}O isotope labeling. We provide direct evidence for the enzymatic regulation of N_2O production by AOA. We found hydroxylamine oxidation contributes substantially to N_2O production, which had not been previously recognized, and that nitrite reduction is not a significant source of N_2O. These findings are important for the interpretation of pathways and regulation of N_2O production in the ocean.

Author contributions: X.S.W., W.Q., and B.B.W. designed research; X.S.W., L.H., H.-X.S., H.S., and S.T. performed research; S.-J.K., and Y.Z. contributed new reagents/analytic tools; X.S.W., L.H., W.Q., and B.B.W. analyzed data; and X.S.W. and B.B.W. wrote the paper with input from all authors.

The authors declare no competing interest.

This article is a PNAS Direct Submission.

[1]To whom correspondence may be addressed. Email: xianhuiw@princeton.edu or bbw@princeton.edu.

This article contains supporting information online at https://www.pnas.org/lookup/suppl/doi:10.1073/pnas.2220697120/-/DCSupplemental.

Published March 8, 2023.

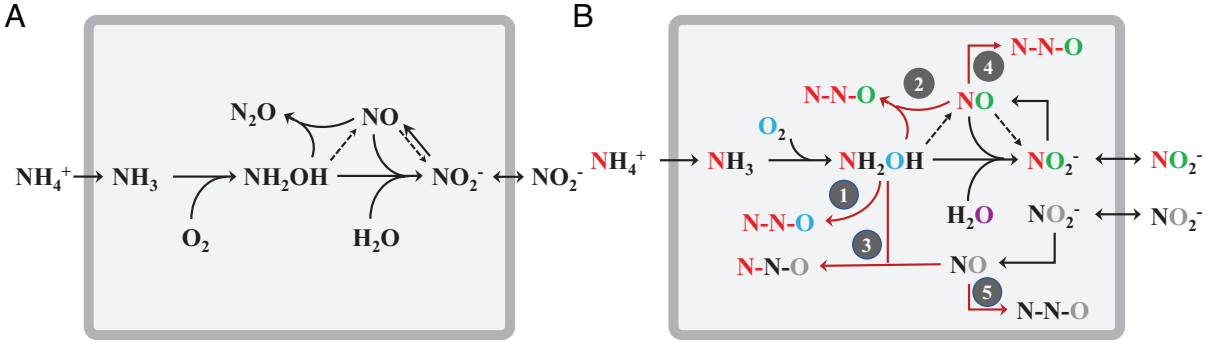

C

Process	N atom source	O atom source	Fraction (%)
1. NH_2OH auto-oxidation	NH_4^+	O_2	38
2. Hybrid pathway using cellular NO_2^-	NH_4^+	O_2, H_2O	22
3. Hybrid pathway using ambient NO_2^-	NH_4^+, ambient NO_2^-	NO_2^-	38
4. Chemo-denitrification using cellular NO_2^-	NH_4^+	O_2, H_2O	<2
5. Chemo-denitrification using ambient NO_2^-	Ambient NO_2^-	NO_2^--	<2

Fig. 1. Summary of N_2O production pathways during marine archaeal ammonia oxidation. (*A*) The hybrid pathway, which combines one N atom from NH_2OH and one from nitrite (either ambient or newly produced inside the cell), has been observed previously (10–12). Black arrows represent known pathways for N atoms; dashed pathways represent hypothesized pathways involving NO. (*B*) Potential N_2O pathways and the N and O atom sources identified in the current study. Five N_2O pathways are identified: 1) NH_2OH oxidation; 2) hybrid pathway a: NH_2OH reaction with NO that was sourced from the reduction of newly produced NO_2^-; 3) hybrid pathway b: NH_2OH reaction with NO that was sourced from ambient NO_2^-; 4) reduction of newly produced NO_2^-; and 5) reduction of ambient NO_2^-. Color of the N and O atoms depicts the sources: red and black denote N atoms from NH_4^+ and ambient NO_2^-, respectively; blue, purple, and gray denote O atoms from O_2, H_2O, and ambient NO_2^-, respectively; green represents O atoms of newly produced NO_2^-, which is a mixture of H_2O and O_2. The gray square denotes the membrane and periplasmic space of the AOA cell. The black arrows represent the ammonia oxidation pathway, the red arrows show the potential N_2O production processes, and the dashed arrows indicate potential pathways that are unresolved in our study. (*C*) Summary of the N, O atom sources of N_2O and the fractional contribution of each pathway during marine archaeal ammonia oxidation with initial NH_4^+: NO_2^- ratio of 1:1.

of the nitrogen (N) atoms (13, 16–18). However, using N isotopes alone is insufficient to distinguish multiple N_2O production pathways that occur simultaneously and to quantitatively estimate the relative contribution of each pathway. For instance, the ^{15}N-NH_4^+ isotope labeling approach cannot completely distinguish N_2O production through NH_2OH oxidation, hybrid formation, or NO_2^- reduction, because all these precursors of N_2O could ultimately be sourced from NH_4^+ during ammonia oxidation. The ^{18}O-labeling approach provides an independent avenue to identify the source of N_2O by tracking the oxygen (O) atom in N_2O. A few studies have used ^{18}O-H_2O to show that the O atom in N_2O can be partly derived from H_2O in lab culture and field studies (9, 19, 20). However, the alternative sources of the O atom in N_2O are still unknown. Importantly, because the O atom source differs among the various N-containing precursors, i.e., NH_2OH, NO_2^-, and NO, dual ^{15}N and ^{18}O isotope labeling is a powerful method to disentangle the complex and interconnected N_2O production pathways in AOA. In this study, using a model marine AOA species *Nitrosopumilus maritimus* strain SCM1 (hereafter refer to as SCM1), we conducted a comprehensive set of dual-isotope labeling incubation experiments to systematically investigate N_2O production kinetics and the associated pathways during archaeal ammonia oxidation under various substrate conditions (*SI Appendix*, Table S1).

Results and Discussion

Kinetics of N_2O Production during Archaeal Ammonia Oxidation. Marine AOA have a remarkably high affinity for NH_4^+, which is consistent with their dominant role in ammonia oxidation to NO_2^- in oligotrophic marine environments (2). However, the effect of NH_4^+ concentrations on N_2O production by AOA remains unknown. If N_2O is primarily generated via abiotic hybrid reactions between intermediates of archaeal ammonia oxidation, N_2O production by AOA may not follow normal enzyme kinetics. We found that both NO_2^- and N_2O production rates varied with NH_4^+ concentration (Experiment 1) and both followed Michaelis-Menten-type kinetics (Fig. 2 *A* and *B*). The apparent half saturation constants ($K_{m(app)}$) for NO_2^- production (220 ± 50 nmol L^{-1} NH_4^+) were comparable to those that were previously determined for ammonia (132 nmol L^{-1} NH_4^+) and oxygen uptake (133 nmol L^{-1} NH_4^+), suggesting all essential enzymatic steps for ammonia oxidation and respiration are highly efficient and tightly coupled at low ammonia concentrations in marine AOA. Likewise, although the maximum rate (V_{max}) for N_2O production (0.97 ± 0.02 amol N $cell^{-1}$ d^{-1}) was more than three orders of magnitude lower than that for NO_2^- production (7.14 ± 0.25 fmol N $cell^{-1}$ d^{-1}), $K_{m(app)}$ values for the two rates were comparably low. The comparable $K_{m(app)}$ values for ammonia during NO_2^- and N_2O production imply that both are controlled by enzyme activity in SCM1 at low NH_4^+ concentrations. This implies that enzyme activity provides the key intermediates NH_2OH and NO for both NO_2^- and N_2O production, i.e., there is no separate completely abiotic reaction that is responsible for N_2O production. The $K_{m(app)}$ for N_2O production is four orders of magnitude lower than the K_m reported for NO production by SCM1 measured during ammonia oxidation (measured at >2 mol L^{-1} NH_4^+) (14). Therefore, the supply of NO is unlikely to be a limiting factor in determining the kinetics of N_2O production, implying a critical role for NH_2OH in determining the observed kinetics.

NH_2OH is enzymatically produced by ammonia monooxygenase and rapidly converted to NO_2^- (15). The tight coupling of its

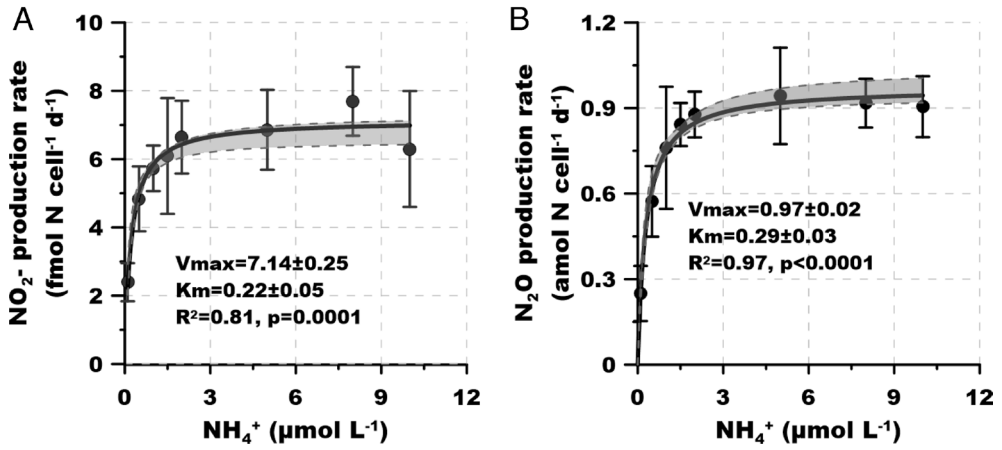

Fig. 2. Experiment 1. Kinetics of ammonia oxidation and N_2O production by SCM1. (*A*) Michaelis-Menten-type plot of substrate-dependent rate of ammonia oxidation to NO_2^- (normalized to per cell per day). (*B*) Michaelis-Menten plot of substrate-dependent rate of N_2O production. Error bars represent SD from triplicate samples. The black lines and gray shadows show the Michaelis-Menten type regressions and the 95% CIs, respectively.

production and consumption in AOA species at low NH_4^+ concentrations results in its limiting conversion to N_2O as a side product. However, a small fraction of NH_2OH can escape from being oxidized by the enzymatic reaction, providing the key precursor for N_2O production. For example, only 0.46% of NH_2OH was released during ammonia oxidation by the AOA *Nitrososphaera gargensis* even at very high NH_4^+ concentrations [2 mmol L^{-1} (21)], which is one to two orders of magnitude lower than the reported NO accumulation ratio during ammonia oxidation by SCM1 (14). The similarly high affinities (low K_m) for NO_2^- and N_2O production further suggest that both kinetics were determined by the NH_2OH supply; if the conversion of NH_2OH to NO_2^- was the rate-limiting step, the production of N_2O should increase continuously with the accumulation of NH_2OH. These results suggest that the SCM1-like marine AOA effectively use the trace level NH_4^+ in the vast N-depleted ocean for both NO_2^- and N_2O generation, providing direct evidence for the capability of marine AOA to dominate N_2O production in the ocean and its subsequent release to the atmosphere.

Impact of NH_4^+: NO_2^- Ratio on Pathways of N_2O Production. Both NH_4^+ and NO_2^- are involved in N_2O production by AOA (9, 18), but the rates and pathways might vary depending on relative substrate availability. Therefore, we investigated N_2O production under a wide range of $^{15}NH_4^+$: $^{14}NO_2^-$ ratios (from 0.05 to 10) (Experiments 1 and 2). The ratio of single labeled N_2O to double labeled N_2O ($^{45}N_2O$: $^{46}N_2O$) decreased from 5.82 ± 2.58 to 0.37 ± 0.05 as the $^{15}NH_4^+$: $^{14}NO_2^-$ ratio increased from 0.05 to 10 (Fig. 3*A* and *SI Appendix*, Fig. S1). This dependence on substrate ratio indicates that $^{45}N_2O$: $^{46}N_2O$ ratio is not a constant but is highly variable and implies that more than one pathway contributes to N_2O production in AOA. The strong and significant correlation (R^2 = 0.97, P < 0.0001) between the $^{45}N_2O$: $^{46}N_2O$ ratio and substrate $^{15}NH_4^+$: $^{14}NO_2^-$ ratio implies that the relative contributions of different pathways to N_2O production and the source of the N atoms in N_2O should vary with NH_4^+: NO_2^- ratio in the environment (Fig. 3*B*).

NH_4^+ and NO_2^- are highly dynamic nitrogen cycle components that rarely accumulate in the global ocean. However, NH_4^+ and NO_2^- can accumulate in specific regions (e.g., oxygen minimum zones and eutrophic waters) and depths (e.g., NH_4^+ maximum, primary NO_2^- maximum), leading to substantial variation of NH_4^+: NO_2^- ratio in these biogeochemically active marine environments (22). Our data indicate that N_2O can be produced via distinct pathways by marine AOA and sourced from different N atoms in waters with different ratios of NH_4^+: NO_2^-, even though the main source process is always archaeal ammonia oxidation. For example, at the primary NO_2^- maximum where NO_2^- accumulates, the low NH_4^+: NO_2^- ratio might lead to the higher contribution of NO_2^- to N_2O production via the hybrid pathway. In

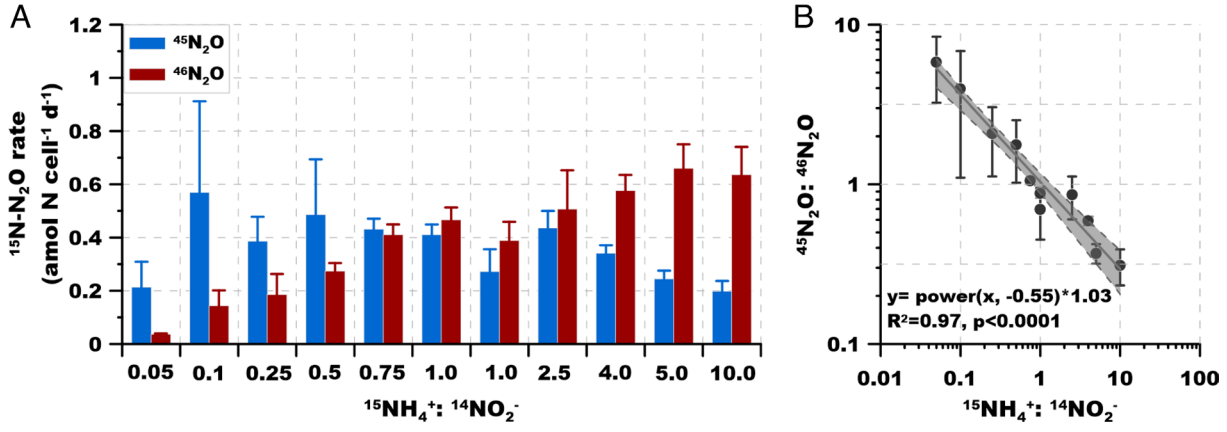

Fig. 3. Experiment 2. ^{15}N-N_2O production and isotope composition under different $^{15}NH_4^+$ $^{14}NO_2^-$ ratios. (*A*) $^{45}N_2O$ (single labeled) and $^{46}N_2O$ (double labeled) production rate under different $^{15}NH_4^+$ and $^{14}NO_2^-$ concentrations (normalized to per cell per day). All of the $^{45}N_2O$ represents hybrid formation. (*B*) Regression between $^{45}N_2O$: $^{46}N_2O$ production rate against $^{15}NH_4^+$ $^{14}NO_2^-$ concentration ratio. Error bars represent SD from triplicate samples.

contrast, at the NH_4^+ maximum and certain hotspots of NH_4^+ supply such as zooplankton excretion or decay of phytoplankton blooms (23), NH_4^+ would dominate N_2O formation under the elevated NH_4^+: NO_2^- ratio. These findings provide new insights in interpreting the natural abundance isotope signature of N_2O in the water column of the global oligotrophic oceans, where a subsurface dual-isotope minimum is consistently observed and has been widely interpreted as resulting from N_2O production via nitrifier-denitrification (24–27). These new data would suggest, however, that low NH_4^+: NO_2^- ratio (i.e., relatively higher NO_2^- concentration) would also lead to the observed dual-isotope minimum by the incorporation of more isotopically depleted NO_2^- by the hybrid pathway during the ammonia oxidation process.

Our results are also important for the interpretation of isotope labeling patterns observed in isotope tracer experiments in the ocean, where production of $^{45}N_2O$ has been generally attributed to the hybrid N_2O formation pathway (one N from NH_4^+, one N from NO_2^-). We suggest that $^{46}N_2O$ could also be partially hybrid, from the combination of $^{15}NH_4^+$ and newly produced $^{15}NO_2^-$. The contribution of the hybrid pathway would be underestimated by ignoring $^{46}N_2O$ production. However, our results cannot fully explain the high fraction of $^{45}N_2O$ production (i.e., >70%) in the ocean (24, 28–30), nor the finding that the $\%^{46}N_2O$ is insensitive to short-term experimental NO_2^- enrichment (31) (comparison to field observations; *SI Appendix*, Text 1). Nevertheless, the variable N_2O atom composition by SCM1 under different NH_4^+: NO_2^- ratio provides new insights into marine N_2O pathways and interpretation of its isotope composition. These pathways and the relative contributions of N and O from multiple sources are explored in experiments described below.

Contribwutions of NH_4^+ and NO_2^- to N_2O Production. The potential pathways and relative contributions of the two substrates, NH_4^+ and NO_2^-, via various pathways of N_2O formation in AOA were explored using multiple tracer combinations (Experiment 3). NH_4^+ and NO_2^- concentrations were controlled by adding the substrates to cells that had first been washed and resuspended in substrate-free fresh medium. When $^{15}NH_4^+$ was added without $^{14}NO_2^-$, double labeled $^{46}N_2O$ was the main product (93.4 ± 10.1% of the total labeled N_2O production rate) (Fig. 4*A*). $^{15}NH_4^+$ was the only N source in the experiment, so the small production of $^{45}N_2O$ (6.6% of the total labeled N_2O production) can be attributed to trace amounts of intracellular $^{14}NH_4^+$ and/ or $^{14}NO_2^-$, or to carry over from the inoculum. When equimolar amounts of $^{15}NH_4^+$ and $^{14}NO_2^-$ were provided, the fractional contribution of $^{45}N_2O$ increased to 28.9%, indicating that ambient NO_2^- is involved in $^{45}N_2O$ production, although the labeled N_2O pool was still primarily $^{46}N_2O$. This hybrid N_2O formation indicates involvement of ambient NO_2^- in N_2O production, but the process varies among AOA strains (18) and with substrate ratio (Fig. 3*B*). Newly produced (presumably intracellular, or at least in the pseudo-periplasmic space) and ambient NO_2^- might both be involved in N_2O hybrid formation (pathways 2, 3 in Fig. 1*B*). Total labeled N_2O (combined $^{45}N_2O$ and $^{46}N_2O$) production rate in the $^{15}NH_4^+$ tracer incubation (8.7 ± 0.7 nmol N L^{-1} d^{-1}, Fig. 4*A*) was comparable to the rate in the $^{15}NH_4^+$ + $^{14}NO_2^-$ incubation (9.6 ± 1.5 nmol N L^{-1} d^{-1}, Fig. 4*B*), indicating no discernible difference between the effects of ambient and newly produced NO_2^- on N_2O production rate by SCM1.

^{15}N-labeled N_2O production from $^{15}NO_2^-$ tracer was negligible (0.3 ± 0.2 nmol N L^{-1} d^{-1}) in the absence of NH_4^+ (Fig. 4*C*). By comparison, when $^{14}NH_4^+$ was added with $^{15}NO_2^-$, the ^{15}N-labeled N_2O production rate increased significantly to 2.6 ± 0.3 nmol N L^{-1} d^{-1} ($P < 0.001$), which is strong evidence for a hybrid N_2O formation mechanism that involves both intermediates from ammonia oxidation and NO_2^- reduction (Fig. 4*D*). It is not surprising that N_2O production rate decreased greatly in the absence of NH_4^+, as NH_4^+ is the substrate for energy generation and the source of the key N_2O precursor NH_2OH. Thus, N_2O can be produced from NH_4^+ alone in the absence of NO_2^-, but N_2O cannot be produced from NO_2^- alone. When NH_4^+ is present, however, NO_2^- contributes to N_2O formation via a hybrid pathway. In contrast to the $^{15}NH_4^+$ tracer experiment, $^{45}N_2O$ dominated the ^{15}N-N_2O pool in the $^{15}NO_2^-$ + $^{14}NH_4^+$ incubation (92.1 ± 16.8%). The small fraction (7.9 ± 3.4%) of $^{46}N_2O$ detected in this treatment indicated a minor contribution of the chemo-denitrification-like pathway (i.e., both N atoms from NO_2^-, pathways 4, 5 in Fig. 1*B*) to N_2O production (Fig. 4*D*) (13). However, the $^{46}N_2O$ production rate from $^{15}NO_2^-$ measured here was two orders of magnitude lower than rates measured when external oxygen was exhausted (5 to 22 nmol L^{-1} h^{-1}) (17), indicating production of N_2O in AOA by the proposed NO_2^- reduction-NO dismutation pathway is restricted to anoxic conditions.

The Role of NH_2OH as Key Precursor for N_2O Production. Although NH_2OH is not an important N source in the marine environment (its reactivity guarantees a very low ambient concentration) (32), it is a critical intracellular intermediate in archaeal ammonia oxidation and N_2O production. Experiments using $^{15}NH_2OH$ and $^{15}NO_2^-$ + $^{14}NH_2OH$ were used to explore the pathways by

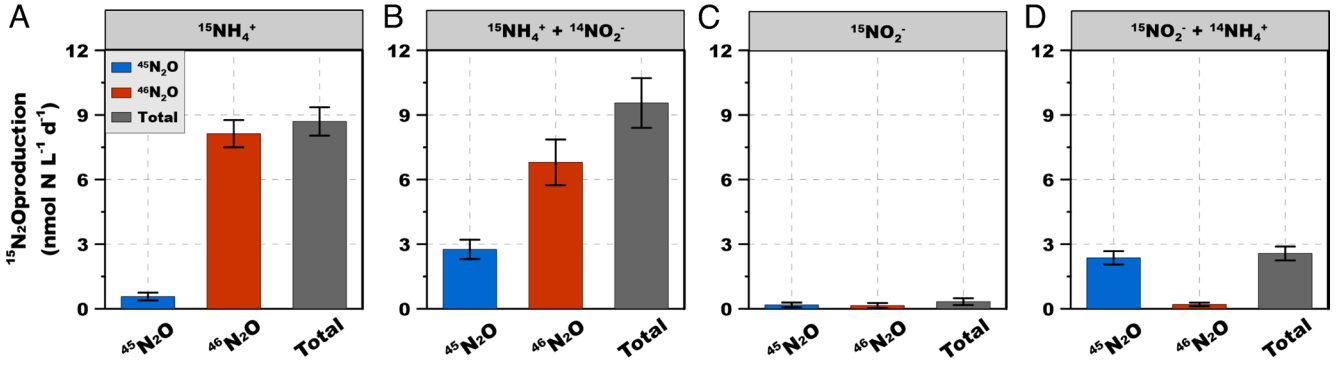

Fig. 4. Experiment 3. ^{15}N-N_2O production during $^{15}NH_4^+$ and $^{15}NO_2^-$ labeling incubations using viable cells. (*A*–*D*) ^{15}N labeled N_2O production rate from $^{15}NH_4^+$, $^{15}NH_4^+$ + $^{14}NO_2^-$, $^{15}NO_2^-$, and $^{15}NO_2^-$ + $^{14}NH_4^+$ labeling incubations, respectively. Error bars represent SD from triplicate incubations. Total N_2O refers to total labeled N_2O ($^{45}N_2O$ + $^{46}N_2O$). Approximately, 6 nmol N L^{-1} d^{-1} $^{44}N_2O$ must have been produced in the $^{15}NO_2^-$ + $^{14}NH_4^+$ incubation (*D*), but the amount of $^{44}N_2O$ could not be determined in these experiments due to lack of sensitivity in small volume incubations. $^{44}N_2O$ would not have been present in the other three experiments because in *A* all the NH_4^+ was labeled; in *B* we have shown that N_2O cannot be formed from NO_2^- alone, and *C* all the NO_2^- was labeled.

which NH_2OH participates in N_2O production during ammonia oxidation (Experiment 4). Notably, here we used 1 μmol L^{-1} of NH_2OH concentration, which was two orders of magnitude lower than previous studies that explored N_2O pathways by AOA (i.e., 200 μmol L^{-1}) (13), thus closer to environmental concentrations but also ensuring the sensitivity of the assays to probe the potential mechanisms. Moreover, no discernible difference was observed for NO_2^- production with or without NH_2OH amendment, suggesting no detectable inhibition of 1 μmol L^{-1} of NH_2OH on archaeal ammonia oxidation ($P > 0.05$) (SI *Appendix*, Fig. S2).

$^{45}N_2O$ increased slowly but continuously over 12 h from tracer $^{15}NO_2^-$ in viable cells, while no discernible $^{46}N_2O$ accumulation was detected (Fig. 5*A*). $^{14}NH_2OH$ added with $^{15}NO_2^-$ stimulated $^{45}N_2O$ production from $^{15}NO_2^-$ in viable cells, indicating $^{14}NH_2OH$ was directly involved in the reaction with $^{15}NO_2^-$ to produce hybrid $^{45}N_2O$ (Fig. 5*B*). In contrast, $^{45}N_2O$ production nearly stopped after removing the cells by filtration. The fact that the viable cells produced more $^{45}N_2O$ from the $^{15}NO_2^-$ tracer than the filtrate indicates that cellular metabolism facilitated N_2O production from the hybrid pathway, and that abiotic formation rate of N_2O by NO_2^- and NH_2OH was low (Fig. 5*C*).

Much higher labeled N_2O production rates occurred in incubations supplemented with $^{15}NH_2OH$ (Fig. 5 *D* and *E*) than in incubations supplemented with either $^{15}NO_2^-$ alone or $^{15}NO_2^-$ + $^{14}NH_2OH$, despite the concentration of $^{15}NO_2^-$ (10 μmol L^{-1}) being tenfold higher than $^{15}NH_2OH$ (1 μmol L^{-1}), demonstrating active involvement of NH_2OH in N_2O production. In the presence of viable cells, both $^{45}N_2O$ and $^{46}N_2O$ were produced (Fig. 5*D*), while for the filtrate, only $^{46}N_2O$ production was observed ($^{45}N_2O$ accounted for <5% of the total labeled N_2O production) (Fig. 5*E*). The comparable $^{46}N_2O$ production between viable cell and filtrate groups indicated that $^{46}N_2O$ was mainly produced via abiotic NH_2OH oxidation, and NO_2^- is not involved in that reaction. In contrast, viable cells are needed for the production of $^{45}N_2O$ from $^{15}NH_2OH$ and $^{14}NO_2^-$, suggesting the hybrid reaction may require enzymatic activity to produce NO from NO_2^-. Therefore, it appears that the ambient NO_2^- can enter the periplasmic space of the cell for the production of NO that is most likely catalyzed by a putative periplasmic copper-containing nitrite reductase (10, 11). These results indicate the central role of NH_2OH as a precursor of N_2O (pathways 1, 2, 3, and 4 in Fig. 1*B*). Moreover, the co-production of $^{45}N_2O$ and $^{46}N_2O$ from $^{15}NH_2OH$ shows that hybrid N_2O formation and oxidation of NH_2OH both contributed to N_2O production in viable cells. Note that the high affinity for NH_4^+ and the typical dependence of N_2O production rate on NH_4^+ concentration (Experiment 1) implicate enzymatic control of N_2O production, even though the last step in both pathways (hybrid and NH_2OH oxidation) is abiotic.

Taking all the results with ^{15}N-labeled substrates together, these findings demonstrate that N derived from both NH_4^+ and NO_2^- is involved in N_2O production by AOA, but that NH_4^+ is the major N source. Under the initial NH_4^+: NO_2^- ratio of 1:1, NH_4^+ accounts for ~85% of N atoms to N_2O. Paired analysis of $^{45}N_2O$: $^{46}N_2O$ further implied that an additional N_2O formation pathway solely sourced from NH_4^+ was required to explain the dominance

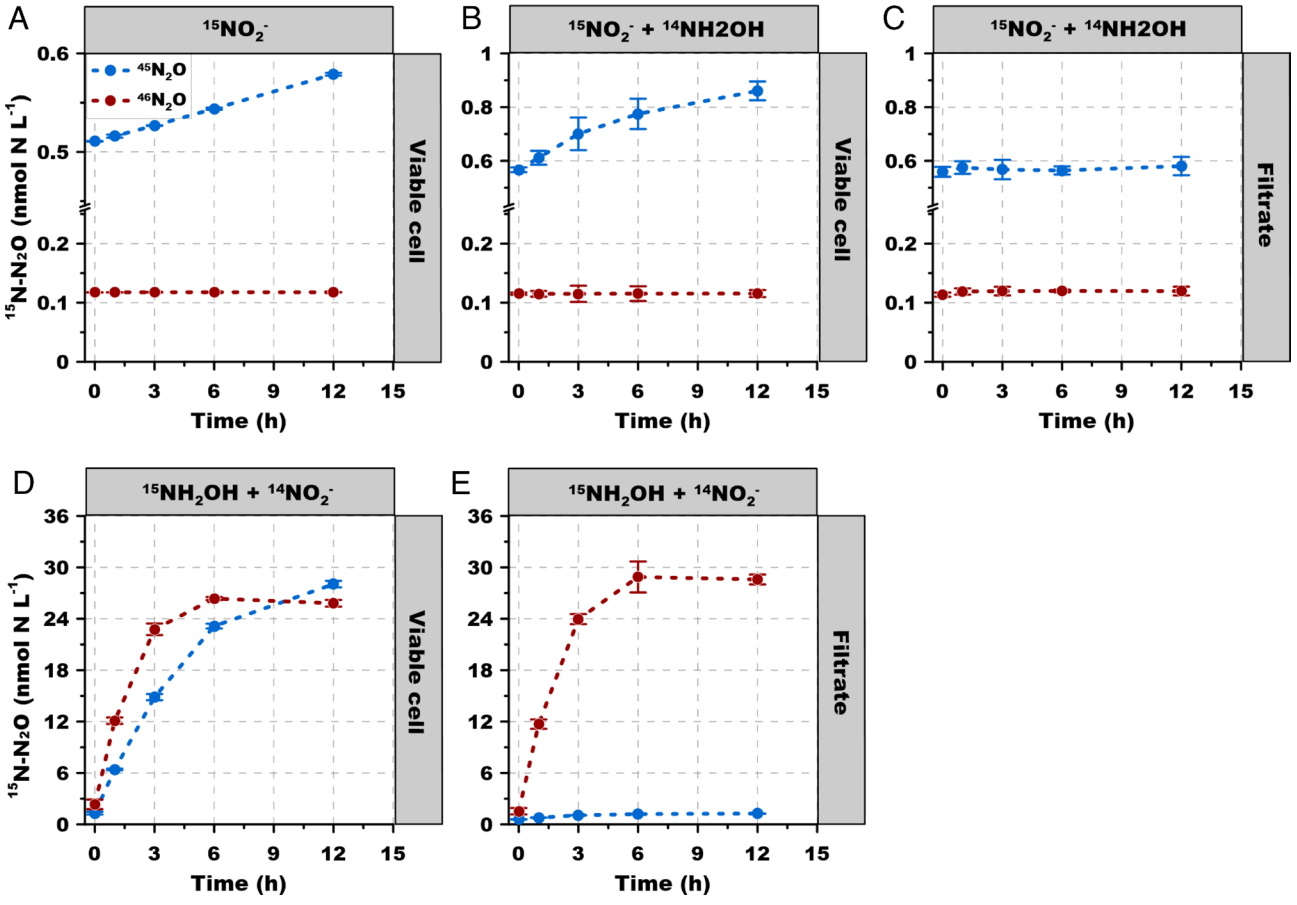

Fig. 5. Experiment 4. ^{15}N-N_2O production from NH_2OH. ^{15}N labeled N_2O production rate from (*A*) viable cells with $^{15}NO_2^-$ tracer (10 μmol L^{-1}); (*B*) viable cells with $^{15}NO_2^-$ (10 μmol L^{-1}) + $^{14}NH_2OH$ (1 μmol L^{-1}); (*C*) filtrate with $^{15}NO_2^-$ (10 μmol L^{-1}) + $^{14}NH_2OH$ (1 μmol L^{-1}); (*D*) viable cells with $^{15}NH_2OH$ (1 μmol L^{-1}) + $^{14}NO_2^-$ (50 μmol L^{-1}); (*E*) filtrate with $^{15}NH_2OH$ (1 μmol L^{-1}) + $^{14}NO_2^-$ (50 μmol L^{-1}). Error bars represent SD from triplicate samples.

of NH_4^+ as the source of N atoms in N_2O. Thus, apart from the hybrid formation pathway, NH_2OH oxidation might be an important and previously overlooked pathway that contributes to archaeal N_2O production. However, it is difficult to discriminate all the associated pathways and to quantify the contributions of each process using N isotopes alone, because all N atoms in N_2O precursors could be directly or indirectly sourced from NH_4^+.

Tracing the O in N_2O: Contributions of H_2O, O_2, and NO_2^- as the Source of O in N_2O. ^{18}O leaves footprints in N_2O and NO_2^- that are independent of ^{15}N and can thus provide further information on the pathways to N_2O. We developed a comprehensive set of ^{18}O-labeling experiments to determine the source of O atoms in both NO_2^- and N_2O, and to quantify potential N_2O production pathways from H_2O, NO_2^-, and O_2 (Experiment 5). The isotopic enrichment of $\delta^{18}O$-NO_2^- showed an approximately linear increase over time in the 24 h abiotic O atom exchange experiment, i.e., from ^{18}O-H_2O in the absence of viable cells (Fig. 6*A*). The measured values of $\delta^{18}O$-NO_2^- agreed well with the amount of $\delta^{18}O$-NO_2^- predicted using an exchange rate constant of 0.117 (33) under the experimental conditions (pH: 7.8; temperature: 30°C).

This correction for abiotic O atom exchange was applied to determine the $\delta^{18}O$ of the produced NO_2^- in incubations with viable cells. O atoms from both H_2O and O_2 were incorporated into NO_2^- during archaeal ammonia oxidation (and the amount of $\delta^{18}O$-NO_2^- was proportional to the amount of labeled substrate in both ^{18}O-H_2O and ^{18}O-O_2 labeling incubations) (Fig. 6 *B* and *C*). The slope of $\delta^{18}O$-NO_2^- vs. $\delta^{18}O$-H_2O (63 ± 3%) was significantly greater than the slope of $\delta^{18}O$-NO_2^- vs. $\delta^{18}O$-O_2 (26 ± 2%) ($P < 0.001$). The significantly higher contribution of H_2O than O_2 to the O atoms in NO_2^- is consistent with the hypothesis that NH_2OH and NO act as co-substrates to produce two molecules of NO_2^-. Then one NO_2^- molecule is reduced back to NO and another O atom from H_2O is incorporated into NO_2^- (13). Alternatively, an intracellular O atom exchange could occur during NO_2^- production by AOA (*SI Appendix*, Text 2).

$\delta^{18}O$ of the produced N_2O increased with increasing $\delta^{18}O$-H_2O, $\delta^{18}O$-O_2 and $\delta^{18}O$-NO_2^-, indicating that O atoms from all three potential sources were incorporated into N_2O (Fig. 6 *D*–*F*) with different contributions. Interestingly, in contrast to the O atom source structure in NO_2^-, O_2 contributed the largest fraction of O atoms to N_2O (44 ± 2%), followed by NO_2^- (30 ± 3%) and H_2O (14 ± 1%). Because the O atoms in NH_2OH are sourced from O_2 and no further exchange occurs between NH_2OH and H_2O (34), the fact that O_2 (via NH_2OH) contributed most to O atoms in N_2O supports our finding of a substantial role for NH_2OH oxidation in producing N_2O (pathway 1 in Fig. 1*B*). The incorporation of O atoms from NO_2^- and H_2O into N_2O indicated internally produced and externally added (ambient) NO_2^- can both be involved in N_2O production. In the absence of known nitric oxide reductase catalyzing NO reduction to N_2O through nitrifier-denitrification, potential N_2O pathways associated with NO_2^- in marine AOA include abiotic NO_2^- reduction (chemo-denitrification-like) and hybrid formation. However, our $^{15}NO_2^-$ labeling incubations showed that NO_2^- was involved in N_2O production only in the presence of NH_4^+, and NO_2^- alone did not contribute substantially to N_2O production (Fig. 4 *C* and *D*). Therefore, hybrid formation is the dominant pathway by which NO_2^- contributes to N_2O production.

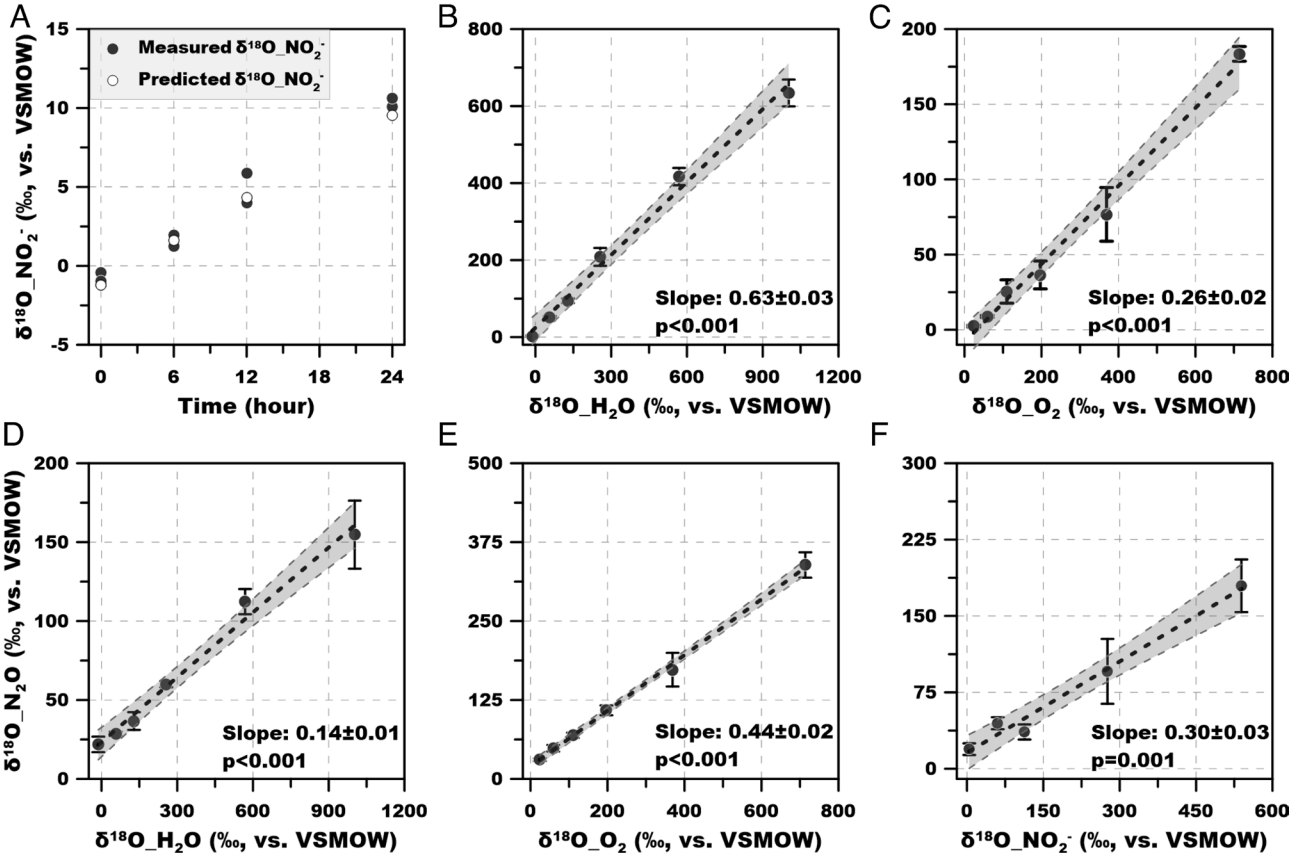

Fig. 6. Experiment 5. $\delta^{18}O$ of the produced NO_2^- and N_2O during the 24 h ^{18}O-labeling incubations. (*A*) Change of $\delta^{18}O$-NO_2^- due to abiotic O atom exchange. (*B* and *C*) $\delta^{18}O$ of the produced NO_2^- in ^{18}O-H_2O and ^{18}O-O_2 labeling experiments. (*D*–*F*) $\delta^{18}O$ of the produced N_2O in ^{18}O-H_2O, ^{18}O-O_2, and ^{18}O-NO_2^- labeling experiments, respectively. Dashed lines denote the best linear regression, and gray shadow represents 95% CIs. Error bars represent SD from triplicate samples.

Moreover, the incorporation of O atoms from H_2O and ambient NO_2^- further revealed that during hybrid formation, O atoms in NO_2^- or NO, rather than NH_2OH, were retained in the N_2O molecule. If the O atom was sourced from NH_2OH during the hybrid process, all the O atoms should be contributed by O_2. The incorporation of the O atom from ambient NO_2^- into N_2O also shows that at least some NO was produced via NO_2^- reduction, as previously hypothesized (11, 14).

Quantifying Multiple N_2O Sources during Archaeal Ammonia Oxidation. The dual-isotope labeling method enabled us to fully resolve multiple N_2O production pathways in AOA. Combining results from ^{15}N and ^{18}O-labeling incubations (Experiments 3 to 5), we can quantitatively estimate the fractional contribution of the five potential N_2O production pathways (Fig. 1*B*). NO_2^- reduction (pathways 4 and 5) is an insignificant N_2O source under aerobic growth conditions when both NH_4^+ and NO_2^- are present in equimolar amounts (Fig. 4). NH_2OH is revealed as the main contributor to N_2O production (Fig. 5) via both hybrid pathway and NH_2OH oxidation. In NH_2OH oxidation (pathway 1), 100% of O atoms in N_2O were sourced from O_2, while in hybrid formation (pathways 2 and 3), the O atom was derived from NO_2^- via reduction to NO. The NH_2OH involved in hybrid N_2O formation contributed an N atom but not the O atom. There were two sources of NO_2^-: the original ambient NO_2^- (100% of O atoms were sourced from ambient NO_2^-) and the NO_2^- newly produced from ammonia oxidation (63% of O atoms from H_2O and 26% from O_2) (Fig. 6). Under these conditions, we calculated the following contributions to O atoms in N_2O: 38.2% from NH_2OH oxidation (pathway 1), 59.8% from the hybrid source (22.2% by pathway 2 and 37.6% by pathway 3), and 2.1% from NO_2^- reduction (pathways 4 and 5) (Fig. 1*C*). This combination best fits the observed results that 14% of O atoms in N_2O were from H_2O and 44% of O atoms were from O_2 under our experimental conditions. Although the fractional contribution of the pathways might vary with various substrate concentrations (i.e., different NH_4^+: NO_2^- ratios), the comprehensive ^{15}N-^{18}O dual-isotope labeling technique developed here provides a novel avenue to disentangle and quantify the relative contribution of multiple pathways to N_2O production in both lab and field studies.

Archaeal ammonia oxidation is the primary source of marine N_2O, yet the mechanistic understanding of archaeal N_2O production remains elusive. We present the first study determining the kinetics of archaeal N_2O production and provide strong evidence of the capability of marine AOA in producing N_2O at trace levels of NH_4^+, supporting their dominant role in contributing to N_2O production in the ocean. We further show a direct control of NH_4^+ and NO_2^- concentrations on the sources of N_2O, providing new insights into understanding the varying isotope composition of N_2O in the ocean. The increased incorporation of N and O atoms from NO_2^- into N_2O by marine AOA at low NH_4^+: NO_2^- ratios suggests a new mechanism for interpreting the ubiquitous N_2O isotope minimum without the need to invoke nitrifier-denitrification by AOB, which are rarely detected in the oligotrophic open ocean. Our comprehensive dual ^{15}N-^{18}O-labeling techniques identify a substantial contribution of NH_2OH oxidation to archaeal N_2O production that was previously not recognized. These explicit descriptions of the N_2O production pathways and kinetics in AOA should improve our understanding of marine N_2O production, and the multiple N and O atom sources of N_2O identified here should inform biogeochemical models that aim to resolve the marine nitrogen cycle and constrain the air-sea N_2O flux. Moreover, our dual-isotope labeling technique could be applied in combination with manipulative experiments, such as temperature, pH, and dissolved oxygen (DO), to explore rates and pathways of archaeal N_2O production in response to ocean warming, acidification and deoxygenation.

Materials and Methods

SCM1 Cultivation and Isotope Labeling Incubation. *N. maritimus* strain SCM1 was cultured in 4-(2-hydroxyethyl)-1-piperazineethanesulfonic acid (HEPES) buffered Synthetic Crenarchaeota Medium (SCM) (pH: ~7.8) at 30 °C in the dark following Qin et al. (2014) (35). Six sets of incubations were carried out (*SI Appendix*, Table S1). The SCM1 cells were grown and maintained in 2-L bottles containing 600 mL SCM for the preservative test and experiments 3 to 5 and were grown in 100-mL bottles containing 40 mL SCM for experiments 1 to 2. The medium contains FeNaEDTA and other trace metals including, Cu, Ni, Zn, and Co. The approximate concentrations of the trace metals can be found in Amin et al. (2013) (36). The medium was supplemented with NH_4Cl at different initial concentrations for each of the experiments: Initial concentrations were 1,000 μmol L^{-1} in the preservative test experiment, 500 μmol L^{-1} in experiments 3 and 5, 200 μmol L^{-1}in experiment 1 and 2, and 100 μmol L^{-1} in experiments 4. Growth was monitored both by measuring NO_2^- concentration and NH_4^+ consumption and by performing cell counts using flow cytometry (Accuri C6, BD Biosciences). After determining the best strategy for terminating the incubation to preserve the concentration and isotopic content of analytes (Preservative Test), the five experimental incubations were carried out to 1) test the kinetic response of N_2O production during SCM1 ammonia oxidation; 2) examine the impact of NH_4^+: NO_2^- substrate ratio on the pathways and composition of N atoms in N_2O; 3) track N atom sources through ^{15}N labeling experiments; 4) test the contribution of ambient NH_2OH to N_2O production; and 5) track O atom sources through multiple ^{18}O-labeling experiments. All labeling incubation experiments were performed using mid- to late-exponential phase cultures.

Preservative test. A total of ~1.0 L of culture was collected and aliquoted into two groups in the mid-exponential phase: 1) viable cells and 2) killed control (autoclaved at 120°C for 30 min and cooled overnight). In each group, each ^{15}N tracer ($^{15}NH_4^+$ and $^{15}NO_2^-$, 99% ^{15}N, Cambridge, United States) was added to separate bottles to a concentration of 50 μmol L^{-1}. For the viable cells, one additional treatment (100 μmol L^{-1} of $^{15}NO_3^-$, 98% ^{15}N, Cambridge, United States) was performed. After tracer addition, 10 mL of sample was dispensed into triplicate 20-mL serum bottles and sealed with 20-mm butyl stoppers and aluminum crimp seals (Wheaton, United States). Two preservatives (20 μL of saturated $HgCl_2$ and 500 μL of 10 mol L^{-1} of NaOH) were used to compare the effect of preservatives on terminating biological activity and archaeal N_2O production. For the viable cells, the incubations were performed at 30°C in the dark and terminated at 0 and 24 h. For the autoclaved samples, the preservatives were added only at 0 h. All incubations were performed in triplicate. Our results showed that $HgCl_2$ induces artifacts of N_2O production from pathways involving NO_2^-. Such artifacts are negligible when using NaOH as a preservative (*SI Appendix*, Fig. S3 and Text 3). Thus, NaOH was chosen as the preservative for all further experiments.

Experiment 1: Kinetic test. When all amended NH_4^+ (200 μmol L^{-1}) was completely consumed (i.e., below the substrate threshold of SCM1, ~10 nmol L^{-1} NH_4^+), 1% inoculum was transferred into NH_4^+ free fresh medium supplemented with labeled tracers. The initial cell abundance was around 1.39 × 10^5 cells ml^{-1}, which is comparable to AOA cell abundance in the ocean, and initial carry over $^{14}NO_2^-$ concentration was ~2 μmol L^{-1}. A total of eight $^{15}NH_4^+$ concentrations (0.1, 0.5, 1, 1.5, 2, 5, 8, 10 μmol L^{-1}) were used for the kinetic test. Immediately after tracer amendment, 50 mL aliquots of sample were dispensed into 60-mL serum bottles and sealed with 20-mm butyl stoppers and aluminum crimp seals (Wheaton, United States). The incubation was performed at 30°C in the dark. Depending on the initial $^{15}NH_4^+$ concentration, the incubation was terminated at 0 h, ~2 h (0.1 μmol L^{-1}), ~6 h (0.5 μmol L^{-1}), and ~12 h (>0.5 μmol L^{-1}) by adding 2.5 mL of 10 mol L^{-1} of NaOH. A third time point (~24 h) was also applied for all treatments. However, the third time point was only used for rate calculation in the high NH_4^+ treatments (>1.5 μmol L^{-1}) because the substrate

was nearly completely consumed or exhausted before 24 h in those low substrate treatments. The incubations were carried out in triplicates at each time point.

Experiment 2: Substrate ratio experiment. When 100 μmol L^{-1} of NH_4^+ was consumed, 1% inoculum was transferred into NH_4^+ free medium. The initial cell abundance was around 6.2 × 10^4 cells mL^{-1}. Three NH_4^+: NO_2^- ratios were achieved by adding different amounts of $^{15}NH_4^+$ and $^{14}NO_2^-$ (10 and 1 μmol L^{-1} of NH_4^+ and NO_2^-, 5 and 5 μmol L^{-1} of NH_4^+ and NO_2^-, and 1.5 and 15 μmol L^{-1} of NH_4^+ and NO_2^-, respectively). Immediately after tracer amendment, 40 mL aliquots of sample were dispensed into 60-mL serum bottles and sealed with 20-mm butyl stoppers and aluminum crimp seals (Wheaton, United States). The incubation was performed at 30°C in the dark and terminated by adding 2 mL of 10 mol L^{-1} of NaOH at 0, 6 and 24 h with triplicates at each time point.

Experiment 3: Source of N atoms in N_2O. A total of ~4 L of culture was harvested by gentle filtration onto two 0.2 μm pore size Sterivex filters (Millipore). Immediately after the filtration, the filters were flushed using 2-L fresh substrate-free medium to collect the cells and to remove the high background NH_4^+ (~210 μmol L^{-1}) and NO_2^- (~330 μmol L^{-1}). The cell densities before (4 L original culture) and after the filtration (resuspended in 2 L medium) were 1.15 × 10^7 and 2.10 × 10^7 cells mL^{-1}, respectively, demonstrating a good recovery efficiency (~60%) of the pre-concentration process. The measured ammonia oxidation rate of the washed cells (~16 μmol N L^{-1} d^{-1}) was lower than the rate of unwashed cells measured on the same day (~84 μmol N L^{-1} d^{-1}). This reduced oxidation rate indicates that the manipulation process caused physiological stress on the SCM1 cells and resulted in decreased cellular activity. Nevertheless, the activity of the washed cells was high enough to allow precise measurement of rates of ammonia oxidation and N_2O production in the experiments. The recovered cells were aliquoted into eight acid washed 250-mL PC bottles (Nalgene) and for four groups of tracers ($^{15}NH_4^+$, $^{15}NH_4^+$ + $^{14}NO_2^-$, $^{15}NO_2^-$, $^{15}NO_2^-$ + $^{14}NH_4^+$). Immediately after tracer amendment, 10 mL aliquots of sample were dispensed into 20-mL serum bottles and sealed with 20-mm butyl stopper and aluminum crimp seals (Wheaton, United States). The incubation was performed at 30°C in the dark and terminated by adding 500 μL of 10 mol L^{-1} of NaOH at 0 and 24 h with triplicates at each time point.

Experiment 4: Role of NH_2OH in N_2O production. Around 1 L of culture was aliquoted into five groups when 50 μmol L^{-1} of NH_4^+ had been oxidized: 1) viable cells amended with $^{15}NO_2^-$ (10 μmol L^{-1}); 2) viable cells amended with $^{15}NO_2^-$ (10 μmol L^{-1}) + $^{14}NH_2OH$ (1 μmol L^{-1}); 3) filtrate (through 0.2 μm PES filter) amended with $^{15}NO_2^-$ (10 μmol L^{-1}) + $^{14}NH_2OH$ (1 μmol L^{-1}); 4) viable cells amended with $^{15}NH_2OH$ (1 μmol L^{-1}); and 5) filtrate (through 0.2 μm PES filter) amended with $^{15}NH_2OH$ (1 μmol L^{-1}). After tracer amendment, 10 mL aliquots of sample were dispensed into 20-mL serum bottles and sealed with 20-mm butyl stoppers and aluminum crimp seals (Wheaton, United States). Time-course incubation (0, 1, 3, 6, 12 h) was carried out for all the groups, and the incubation was performed at 30°C in the dark with triplicates and terminated by adding 500 μL of 10 mol L^{-1} of NaOH at each time point.

Experiment 5: Source of O atoms in N_2O. A total of ~7.2 L of culture was harvested by gentle filtration onto two 0.2-μm pore size Sterivex filters (Millipore). Immediately after the filtration, the filters were back flushed using 2.5 L fresh substrate-free medium to collect the cells and to remove the high background NH_4^+ and NO_2^-. Three groups of tracers ($H_2{}^{18}O$, $^{18}O_2$ and $N^{18}O_2^-$) were used to track the source of the O atom. For the ^{18}O-H_2O labeling experiment, a range of $\delta^{18}O$-H_2O tracer amendments (−13 to 1003‰) were made by adding 0.2 mL of ^{18}O-H_2O stocks with different ^{18}O enrichment into the samples (^{18}O-H_2O stocks were made by mixing the $H_2{}^{18}O$ (99% ^{18}O, Sigma-Aldrich, United States) with distilled deionized H_2O). Similarly, six levels of $\delta^{18}O$-O_2 (24 to 714‰) were made by adding 0.2 mL of ^{18}O-O_2 stocks with different ^{18}O enrichment (^{18}O-O_2 stocks were made by mixing the $^{18}O_2$ (99% ^{18}O, Sigma-Aldrich, United States) with He) into the samples. For the ^{18}O-NO_2^- labeling experiment, five levels of ^{18}O-NO_2^- (4 to 539‰) were made by using the O atom exchange between NO_2^- and $H_2{}^{18}O$. In each treatment, 20 mL of sample was dispensed into 60 -mL serum bottles and sealed with 20-mm butyl stoppers and aluminum crimp seals (Wheaton, United States). The ^{18}O-labeled substrates were injected into the serum bottles. Both the NH_4^+ and NO_2^- were set at 20 μmol L^{-1} in each incubation. For $^{18}O_2$ labeled incubations, after $^{18}O_2$ injection, the bottles were shaken at ~120 rpm for 15 min to equilibrate the $^{18}O_2$ with the dissolved oxygen (DO) in water. The incubation was performed at 30°C in the dark and terminated by adding 1 mL of 10 mol L^{-1} NaOH. A time-course (0, 6, 12, 24 h) incubation was performed in selected tracer treatments ($\delta^{18}O$-H_2O of 129‰; $\delta^{18}O$-O_2 of 110‰; $\delta^{18}O$-NO_2^- of 276‰), and the remaining treatments were terminated at 0 and 24 h; all experiments were performed in triplicates at each time point. An additional set of experiments was performed to examine the rate of abiotic O atom exchange between NO_2^- and H_2O. Briefly, NH_4^+ and NO_2^- were added into ~10 mL of fresh medium to a concentration of 20 μmol L^{-1}, and ~0.1 mL of ^{18}O-H_2O stock was added to get $\delta^{18}O$-H_2O of ~76‰. The incubation was performed at 30°C in the dark and terminated by adding 500 μL of 10 mol L^{-1} of NaOH at 0, 6, 12, and 24 h with duplicates at each time point.

Sample Analysis. The samples for NH_4^+ and NO_2^- concentration measurement were stored at −20°C until analysis. The concentration of NH_4^+ and NO_2^- was measured by colorimetric methods with an AA3 nutrient analyzer or a spectrophotometer. The detection limit for NH_4^+ and NO_2^- was 0.5 and 0.03 μmol L^{-1}, and the analytical precision was better than ±3% and ±1%, respectively (37).

The N_2O samples were stored at 4°C after incubation. For the preservative test and experiments 3 and 4, before measurements, 1.5 nmol of N_2O of known isotope composition ($\delta^{15}N$ = −3.2 ± 0.1‰ relative to air N_2, $\delta^{18}O$ = 36.6 ± 0.1‰ relative to Vienna Standard Mean Ocean Water) was introduced into each serum bottle to provide enough mass for isotopic analysis. For experiments 1, 2, and 5, the samples were measured directly without N_2O carrier addition. Concentration and isotopes of N_2O were measured using a modified Gas Chromatograph-Isotope Ratio Mass Spectrometer (GC-IRMS) (38). Briefly, two needles were used for He pressurization and N_2O purging. For the 20-mL bottles, sample was purged for 6.7 min at a flow rate of 40 mL min^{-1}, and for 60-mL bottles, the purge time was 30 min. The extracted gases were passed through an ethanol trap with dry ice and a chemical trap filled with magnesium perchlorate and Ascarite to remove H_2O and CO_2. N_2O was trapped by liquid nitrogen twice for purification and concentration and then injected into the GC-IRMS with He as carrier gas. N_2O mass was determined by ion peak area [m/z of 44, 45, 46] with standard gases of 199.6, 501.0, and 1,000.2 ppmv N_2O/He, which were run at ten sample intervals. The precision of this method for N_2O mass measurement was estimated to be better than ±3%. $\delta^{15}N$ and $\delta^{18}O$ were calibrated against two reference tanks (R1: 199.6 ppmv N_2O/He, $\delta^{15}N$ = −3.2 ± 0.1‰, $\delta^{18}O$ = 36.6 ± 0.1‰; R2: 501.0 ppmv N_2O/He, $\delta^{15}N$ = −1.6 ± 0.1‰, $\delta^{18}O$ = 36.6 ± 0.3‰). The precision of $\delta^{15}N$ and $\delta^{18}O$ measurements with 2 nmol N_2O reference gas was better than 0.3‰ and 0.4‰, respectively (n = 20) (30). All the samples were measured within 2 wk after the incubations.

After N_2O measurement, the samples were stored at 4°C before further analysis. $\delta^{15}N$ and $\delta^{18}O$ of NO_2^- were determined using the bacterial denitrifier method (39, 40) using a Thermo Finnigan Gasbench system with cryogenic extraction and purification system interfaced to a Delta V^{PLUS} isotopic ratio mass spectrometer. Briefly, ~5 to10 nmol of NO_2^- was quantitatively converted to N_2O using the bacterial strain *Pseudomonas aureofaciens*. The produced N_2O was then introduced to the GC-IRMS through an online N_2O cryogenic extraction and purification system. $\delta^{15}N$ of NO_2^- values were calibrated against NO_3^- isotope standards USGS 34, IAEA N3, and USGS 32; $\delta^{18}O$ of NO_2^- values were calibrated against NO_3^- isotope standards USGS 34, IAEA N3 and USGS 35. The standards were run before, after, and at ten sample intervals. Because of the different branching effect during NO_3^- and NO_2^- reduction by *P. aureofaciens* (i.e., 38‰ vs. 12‰), the $\delta^{18}O$ of NO_2^- was further calibrated by taking account of the branching effect between NO_3^- and NO_2^- (26‰) (41). Accuracy (pooled SD) was better than ±0.2‰ for $\delta^{15}N$ and ±0.4‰ for $\delta^{18}O$ according to analyses of these standards with an injection of a similar amount of NO_3^-. Quality control was also conducted by analyzing laboratory working reference material (3,000 m deep sea water from the South China Sea).

$\delta^{18}O$ of H_2O was measured following McIlvin and Casciotti (2006) (42) using the full exchange of O atom between H_2O and NO_2^- under acidic conditions (pH: 6) at room temperature (~25°C) for 2 wk. $\delta^{18}O$ of NO_2^- was measured as described above, and $\delta^{18}O$ of H_2O was calculated based on the isotope effect of 13‰ between the O atom exchange at room temperature (33).

$\delta^{18}O$ of O_2 was not measured directly. The $\delta^{18}O$ of the $^{18}O_2$ tracer was calculated from the mixing ratio of air (assuming $\delta^{18}O$ air O_2 is 24‰) and $^{18}O_2$ tracer. Briefly, during our incubation, the DO concentration in the medium was near equilibration with air (~244 μmol L^{-1}); thus, a total of ~348 μmol of O_2 was present in the bottle (20 mL of medium and 40 mL of air in the headspace). During the ^{18}O-O_2 labeling incubation, 0 to 12 μL of $^{18}O_2$ gas was introduced into

the headspace and was then fully equilibrated with the water to attain different enrichments of ^{18}O in the incubation, and the $\delta^{18}O$ was then calculated from the $^{18}O/^{16}O$ after tracer addition.

Calculations. Rate of labeled N_2O production from the ^{15}N-labeled substrate was calculated based on the accumulation of $^{45}N_2O$ (single labeled) and $^{46}N_2O$ (double labeled) during the incubation. Total labeled N_2O production rate was defined as the ^{15}N from both $^{45}N_2O$ and $^{46}N_2O$ (Eq. **1**). $^{15}NH_4^+$ oxidation rate was calculated from the increase of $^{15}NO_2^-$.

$$^{15}N - N_2O = {}^{45}N_2O + 2 \times {}^{46}N_2O, \quad [\mathbf{1}]$$

where the total ^{15}N-N_2O includes ^{15}N atom from $^{45}N_2O$ (one ^{15}N atom) and $^{46}N_2O$ (two ^{15}N atoms in each molecule).

$\delta^{18}O$ of the produced N_2O during the incubation was calculated using a two-endmember mixing model (Eq. **2**) (43).

$$\delta^{18}O - N_2O_P = \frac{M_{t24} \times \delta^{18}O_{N_2O_{t24}} - M_{t0} \times \delta^{18}O_{N_2O_{t0}}}{M_{t24} - M_{t0}}, \quad [\mathbf{2}]$$

where $\delta^{18}O$-N_2O_P, $\delta^{18}O$-N_2O_{t24}, and $\delta^{18}O$-N_2O_{t0} denote the $\delta^{18}O$-N_2O value of the net produced N_2O during the ^{18}O-labeling incubation, $\delta^{18}O$-N_2O at the end and beginning of incubation, respectively. M_{t24} and M_{t0} denote the measured N_2O mass at the end and beginning of incubation, respectively.

$\delta^{18}O$ of the produced NO_2^- during the ^{18}O-H_2O and ^{18}O-O_2 incubations was calculated using Eq. **2** after calibrating the abiotic O atom exchange between NO_2^- and H_2O (9, 33). Briefly, the abiotic O atom exchange rate was derived from the time-course experiment using cell-free medium, which was then used to calibrate the contribution of abiotic O atom exchange during our incubation (Eq. **3**). The difference between the measured ^{18}O-NO_2^- and the predicted ^{18}O-NO_2^- by abiotic exchange was then used to calculate the $\delta^{18}O$ of newly produced NO_2^- during the incubation. The slopes of the newly produced $\delta^{18}O$-NO_2^- and $\delta^{18}O$-N_2O against $\delta^{18}O$ of different substrates (H_2O, O_2, NO_2^-) were identified as the fraction contribution of O atom from various substrates to the NO_2^- and N_2O (9, 33).

$$\delta^{18}O_{NO_{2abio}^-} = (\delta^{18}O_{NO_{2t0}^-} - \delta^{18}O_{NO_{2eq}^-}) \times \exp(-k \times t) + \delta^{18}O_{NO_{2eq}^-}, \quad [\mathbf{3}]$$

where $\delta^{18}O$-$NO_2^-{}_{abio}$, $\delta^{18}O$-$NO_2^-{}_{t0}$, and $\delta^{18}O$-$NO_2^-{}_{eq}$ are $\delta^{18}O$ value of NO_2^- at the end, beginning, and the equilibrated NO_2^- with H_2O due to abiotic O exchange. t is the incubation length in hours and k is the rate constant.

Data, Materials, and Software Availability. All data needed to evaluate the conclusions in the paper are deposited in Zenodo database that can be accessed through (https://doi.org/10.5281/zenodo.7378577) (44).

ACKNOWLEDGMENTS. We gratefully acknowledge advice, scientific discussions, and comments on the manuscript from Michael L. Bender. We appreciate Xiangpeng Li, Long Q. Ngo, Li Liu, Junyi Ni, and Tingyuan Liu's assistance during cell culture and harvest, Lili Han for the nutrient measurements, and Sergey Oleynik for maintaining the mass spectrometers at Princeton. This work was funded by the Simons Foundation through award No. 675459 to B.B.W. and was supported by National Natural Science Foundation of China through grants 42125603, 92058204, and 41890802 and by the start-up funding of the University of Oklahoma to W.Q.

Author affiliations: [a]Department of Geosciences, Princeton University, Princeton, NJ 08544; [b]State Key Laboratory of Marine Environmental Science, Xiamen University, Xiamen 361101, China; and [c]Department of Microbiology and Plant Biology, Institute for Environmental Genomics, University of Oklahoma, Norman, OK 73019

1. A. E. Santoro, R. A. Richter, C. L. Dupont, Planktonic marine Archaea. *Ann. Rev. Mar. Sci.* **11**, 131–158 (2019).
2. W. Martens-Habbena, P. M. Berube, H. Urakawa, J. R. de la Torre, D. A. Stahl, Ammonia oxidation kinetics determine niche separation of nitrifying Archaea and Bacteria. *Nature* **461**, 976–979 (2009).
3. E. T. Buitenhuis, P. Suntharalingam, C. Le Quéré, Constraints on global oceanic emissions of N_2O from observations and models. *Biogeosciences* **15**, 2161–2175 (2018).
4. A. Freing, D. W. R. Wallace, H. W. Bange, Global oceanic production of nitrous oxide. *Philos. Trans. R. Soc. Lond. B Biol. Sci.* **367**, 1245–1255 (2012).
5. Q. Ji, E. Buitenhuis, P. Suntharalingam, J. L. Sarmiento, B. B. Ward, Global nitrous oxide production determined by oxygen sensitivity of nitrification and denitrification. *Global Biogeochem. Cy.* **32**, 1790–1802 (2018).
6. C. B. Walker *et al.*, Nitrosopumilus maritimus genome reveals unique mechanisms for nitrification and autotrophy in globally distributed marine crenarchaea. *Proc. Natl. Acad. Sci. U.S.A.* **107**, 8818–8823 (2010).
7. L. Hink *et al.*, Kinetics of NH_3-oxidation, NO-turnover, N_2O-production and electron flow during oxygen depletion in model bacterial and archaeal ammonia oxidisers. *Environ. Microbiol.* **12**, 4882–4896 (2017).
8. W. Qin *et al.*, Influence of oxygen availability on the activities of ammonia-oxidizing archaea. *Environ. Microbiol. Rep.* **9**, 250–256 (2017).
9. A. E. Santoro, C. Buchwald, M. R. McIlvin, K. L. Casciotti, Isotopic signature of N_2O produced by marine ammonia-oxidizing archaea. *Science* **333**, 1282–1285 (2011).
10. J. I. Prosser, L. Hink, C. Gubry-Rangin, G. W. Nicol, Nitrous oxide production by ammonia oxidizers: Physiological diversity, niche differentiation and potential mitigation strategies. *Glob. Chang. Biol.* **26**, 103–118 (2020).
11. L. Y. Stein, Insights into the physiology of ammonia-oxidizing microorganisms. *Curr. Opin. Chem. Biol.* **49**, 9–15 (2019).
12. L. Y. Stein *et al.*, Comment on"A critical review on nitrous oxide production by ammonia-oxidizing Archaea" by Lan Wu, Xueming Chen, Wei Wei, Yiwen Liu, Dongbo Wang, and Bing-Jie Ni. *Environ. Sci. Technol.* **55**, 797–798 (2021).
13. J. A. Kozlowski, M. Stieglmeier, C. Schleper, M. G. Klotz, L. Y. Stein, Pathways and key intermediates required for obligate aerobic ammonia-dependent chemolithotrophy in bacteria and Thaumarchaeota. *ISME J.* **10**, 1836–1845 (2016).
14. W. Martens-Habbena *et al.*, The production of nitric oxide by marine ammonia-oxidizing archaea and inhibition of archaeal ammonia oxidation by a nitric oxide scavenger. *Environ. Microbiol.* **17**, 2261–2274 (2015).
15. N. Vajrala *et al.*, Hydroxylamine as an intermediate in ammonia oxidation by globally abundant marine archaea. *Proc. Natl. Acad. Sci. U.S.A.* **110**, 1006–1011 (2013).
16. M. Y. Jung *et al.*, Indications for enzymatic denitrification to N_2O at low pH in an ammonia-oxidizing archaeon. *ISME J.* **13**, 2633–2638 (2019).
17. B. Kraft *et al.*, Oxygen and nitrogen production by an ammonia-oxidizing archaeon. *Science* **375**, 97–100 (2022).
18. M. Stieglmeier *et al.*, Aerobic nitrous oxide production through N-nitrosating hybrid formation in ammonia-oxidizing archaea. *ISME J.* **8**, 1135–1146 (2014).
19. D. M. Kool, C. Müller, N. Wrage, O. Oenema, J. W. Van Groenigen, Oxygen exchange between nitrogen oxides and H_2O can occur during nitrifier pathways. *Soil Biol. Biochem.* **8**, 1632–1641 (2009).
20. N. Wrage, J. W. van Groenigen, O. Oenema, E. M. Baggs, A novel dual-isotope labeling method for distinguishing between soil sources of N_2O. *Rapid Commun. Mass Spectrom.* **19**, 3298–3306 (2005).
21. S. Liu *et al.*, Abiotic conversion of extracellular NH_2OH contributes to N_2O emission during ammonia oxidation. *Environ. Sci. Technol.* **51**, 13122–13132 (2017).
22. N. Gruber, "The marine nitrogen cycle: Overview and challenges" in *Nitrogen in the Marine Environment*, D. G. Capone, D. A. Bronk, M. R. Mulholland, E. J. Carpenter, Eds. (Elsevier, ed. 2, 2008), pp. 1–50.
23. S. Hernández-León, C. Fraga, T. Ikeda, A global estimation of mesozooplankton ammonium excretion in the open ocean. *J. Plankton Res.* **30**, 577–585 (2008).
24. F. Breider *et al.*, Response of N_2O production rate to ocean acidification in the western North Pacific. *Nat. Clim. Chang.* **12**, 954–958 (2019).
25. J. Charpentier, L. Farias, N. Yoshida, N. Boontanon, P. Raimbault, Nitrous oxide distribution and its origin in the Central and Eastern South Pacific Subtropical Gyre. *Biogeosciences* **4**, 729–741 (2007).
26. B. N. Popp *et al.*, Nitrogen and oxygen isotopomeric constraints on the origins and sea-to-air flux of N_2O in the pligotrophic Subtropical North Pacific Gyre. *Global Biogeochem. Cy.* **16**, 1064 (2002).
27. G. L. Zhang *et al.*, Distribution of concentration and stable isotopic composition of N_2O in the shelf and slope of the Northern South China Sea: Implications for production and emission. *J. Geophys. Res. Oceans* **124**, 6218–6234 (2019).
28. C. Frey *et al.*, Regulation of nitrous oxide production in low-oxygen waters off the coast of Peru. *Biogeosciences* **17**, 2263–2287 (2020).
29. Q. Ji, B. B. Ward, Nitrous oxide production in surface waters of the mid-latitude North Atlantic Ocean. *J. Geophys. Res. Oceans* **122**, 2612–2621 (2017).
30. X. S. Wan *et al.*, Epipelagic nitrous oxide production offsets carbon sequestration by the biological pump. *Nat. Geosci.* **16**, 29–36 (2023).
31. C. Frey *et al.*, Kinetics of nitrous oxide production from ammonia oxidation in the Eastern Tropical North Pacific. *Limnol. Oceanogr.* **68**, 424–438 (2022), 10.1002/lno.12283.
32. F. Korth, A. Kock, D. L. Arevalo-Martinez, H. W. Bange, Hydroxylamine as a potential indicator of nitrification in the open ocean. *Geophys. Res. Lett.* **46**, 2158–2166 (2019).
33. C. Buchwald, K. L. Casciotti, Isotopic ratios of nitrite as tracers of the sources and age of oceanic nitrite. *Nat. Geosci.* **6**, 308–313 (2013).
34. K. L. Casciotti, M. McIlvin, C. Buchwald, Oxygen isotopic exchange and fractionation during bacterial ammonia oxidation. *Limnol. Oceanogr.* **55**, 753–762 (2010).
35. W. Qin *et al.*, Marine ammonia-oxidizing archaeal isolates display obligate mixotrophy and wide ecotypic variation. *Proc. Natl. Acad. Sci. U.S.A.* **111**, 12504–12509 (2014).
36. S. A. Amin *et al.*, Copper requirements of the ammonia-oxidizing archaeon *Nitrosopumilus maritimus* SCM1 and implications for nitrification in the marine environment. *Limnol. Oceanogr.* **58**, 2037–2045 (2013).
37. A. Han *et al.*, Nutrient dynamics and biological consumption in a large continental shelf system under the influence of both a river plume and coastal upwelling. *Limnol. Oceanogr.* **57**, 486–502 (2012).

38. M. R. McIlvin, K. L. Casciotti, Fully automated system for stable isotopic analyses of dissolved nitrous oxide at natural abundance levels. *Limnol. Oceanogr.-Meth.* **8**, 54–66 (2010).
39. K. L. Casciotti, D. M. Sigman, M. G. Hastings, J. K. Böhlke, A. Hilkert, Measurement of the oxygen isotopic composition of nitrate in seawater and freshwater using the denitrifier method. *Anal. Chem.* **74**, 4905–4912 (2002).
40. M. A. Weigand, J. Foriel, B. Barnett, S. Oleynik, D. M. Sigman, Updates to instrumentation and protocols for isotopic analysis of nitrate by the denitrifier method. *Rapid Commun. Mass Spectrom.* **30**, 1365–1383 (2016).
41. K. L. Casciotti, J. K. Böhlke, M. R. McIlvin, S. J. Mroczkowski, J. E. Hannon, Oxygen isotopes in nitrite: Analysis, calibration, and equilibration. *Anal. Chem.* **79**, 2427–2436 (2007).
42. M. R. McIlvin, K. L. Casciotti, Method for the Analysis of $\delta^{18}O$ in Water. *Anal. Chem.* **78**, 2377–2381 (2006).
43. B. Fry, Steady state models of stable isotopic distributions. *Isotopes. Environ. Health. Stud.* **39**, 219–232 (2003).
44. X. S. Wan *et al.*, Dataset of SCM1 N2O production. Zenodo (2022). https://doi.org/10.5281/zenodo.7378577. (Deposited 29 November 2022).